

available at www.sciencedirect.comwww.elsevier.com/locate/brainres

**BRAIN
RESEARCH**

Research Report

Predicting synchronous and asynchronous network groupings of hippocampal interneurons coupled with dendritic gap junctions

Tariq Zahid^a, Frances K. Skinner^{a,b,c,d,*}

^aToronto Western Research Institute, University Health Network, Toronto, Ontario, Canada

^bDepartment of Medicine (Neurology), University of Toronto, Toronto, Ontario, Canada

^cDepartment of Physiology, University of Toronto, Toronto, Ontario, Canada

^dIBBME, University of Toronto, Toronto, Ontario, Canada

ARTICLE INFO
Article history:

Accepted 20 December 2008

Available online 10 January 2009

Keywords:

Basket cell

Hippocampus

Gap junction

Compartmental model

Active dendrite

Phase response curve

Weakly coupled oscillator theory

Spike attenuation

Electrical coupling

ABSTRACT

Direct electrical communication between central nervous system (CNS) neurons including those in the hippocampus is well-established. This form of communication is mediated by gap junctions and it is known that this coupling is important for brain rhythms such as gamma (20–80 Hz) which occur during active behavioural states. It is also known that gap junctions are present at several locations along the dendrites of hippocampal interneurons including parvalbumin-positive basket cell types. Weakly coupled oscillator theory, which uses phase response curves (PRCs), has been used to understand and predict the dynamics of electrically coupled networks. Here we use compartmental models of hippocampal basket cells with different levels of basal and apical spike attenuation together with the theory to show that network output can be broken down into three groupings: synchronous, asynchronous and antiphase-like patterns. Moreover, quantified PRCs can be used as a rule of thumb to determine the occurrence of a particular grouping under weak coupling conditions, which in turn implies that spike delays are critical factors in determining network output. In moving beyond weak coupling to encompass the full physiological regime of coupling strengths with network simulations, we note that it is important to be able to differentiate between these different groupings as it affects how the network responds with modulation. Specifically, an asynchronous grouping provides more dynamic richness as a larger range of phase-locked states can be expressed with strength changes. From a functional viewpoint it may be that modulation of electrically coupled networks are key to controlling cell assemblies that contribute to information coding brain substrates.

© 2009 Elsevier B.V. All rights reserved.

1. Introduction

Communication between central nervous system (CNS) neurons occurs chemically via inhibitory and excitatory synapses, and electrically via gap junctions. Whereas

synapses mediate a slower mode of signal transmission, gap junctions provide a means of direct and fast communication believed to be important in producing synchronous network activities (Hormuzdi et al., 2004). A gap junction channel consists of 12 connexin (Cx) proteins, six on the

* Corresponding author. Toronto Western Hospital, 399 Bathurst St. MP13-317, Toronto, Ontario, Canada M5T 2S8. Fax: +1 416 603 5745. E-mail address: fskinner@uhnres.utoronto.ca (F.K. Skinner).

presynaptic side and six on the postsynaptic side, and is formed when the membranes of two cells are close enough together to form a direct channel through which particles can flow. These connections consist of clusters of channels that are not static pores but can open and close, being modulated by age, pH, phosphorylation and other factors (Connors and Long, 2004). The physiological range of gap junction connections is 10–3000 pS based on a unitary gap junction conductance of 10–300 pS and 1–10 gap junction channels per electrical connection (Galarreta and Hestrin, 2001; Srinivas et al., 1999). Of the different types of Cx proteins, Cx36 gap junction proteins are found between interneurons or inhibitory cells in the CNS (Meier et al., 2002; Parenti et al., 2000; Söhl et al., 2005; Srinivas et al., 1999).

Interneurons have diverse characteristics and they make critical contributions to rhythmic activities in particular and distinct ways (Buzsáki, 2006 (chp.3); McBain and Fisahn, 2001). For example, parvalbumin-positive (PV+) inhibitory basket cells fire preferentially on the descending phase of hippocampal theta oscillations which occur during movement and exploration (Klausberger et al., 2003). One of the most characteristic patterns of the awake brain is gamma oscillations (30–80 Hz) which have been recorded in many brain regions including the hippocampus (Buzsáki, 2006 (chp 9)). Basket cells in the hippocampus form mutually inhibitory networks (Sik et al., 1995) and it is clearly the case that they are major players in producing gamma rhythms both *in vitro* and *in vivo* (e.g., Gloveli et al., 2005; Hajos et al., 2004; Tukker et al., 2007). These basket cells target perisomatic regions of the pyramidal cell and thus can exert significant control over their output. Furthermore, network models incorporating experimentally derived synaptic characteristics produce robust and coherent gamma oscillations (Bartos et al., 2007), thus suggesting that synchronous output from basket cell networks are important contributors to gamma rhythms.

Gap junction coupling contributes to mechanisms underlying gamma generation in the hippocampus (e.g., Csicsvari et al., 2003), and it is notable that gamma oscillations are selectively impaired in Cx36 knockout mice (Buhl et al., 2003). In addition to inhibitory synapses, PV+ basket cells are electrically coupled through gap junctions at multiple locations between their apical and basal dendrites (Fukuda and Kosaka, 2000; Bartos et al., 2001). Interestingly, axo-axonic (or chandelier) and bistratified inhibitory cell types are also endowed with Cx36 dendrodendritic gap junctions (Baude et al., 2007) and exhibit significant gamma modulation *in vivo* (Hajos et al., 2004). This suggests that dendritic gap junctions on different inhibitory cell types may play important roles in shaping network gamma output. Given this, it is essential to understand how non-proximally located gap junctions contribute to producing synchronous output in these types of inhibitory cell networks. However, due to the high degree of technical difficulty in recording from dendrites of particular interneurons, the inability to both record from and identify the gap junction location on a given interneuron, and the inability to experimentally control all system parameters, models and theory are needed to provide insight and understanding, and to guide and suggest experiments. For this, we need not only to consider compartmental models, but also to consider

models that incorporate characteristics that are specific to the inhibitory cell type.

Several theoretical and modeling studies have clearly shown that cellular, intrinsic properties affect the particular network patterns that arise in electrically coupled networks (Chow and Kopell, 2000; Lewis and Rinzel, 2003; Pfeuty et al., 2003; Saraga et al., 2006; Sherman and Rinzel, 1992), and in networks with both electrical and inhibitory coupling (Gao and Holmes, 2007; Kopell and Ermentrout, 2004; Lewis and Rinzel, 2003; Pfeuty et al., 2005; Skinner et al., 1999). Proximal and distal connections on dendrites can have opposite effects on network output, and this can be modulated by intrinsic properties of the cell (Crook et al., 1998; Gansert et al., 2007; Lewis and Rinzel, 2004; Saraga and Skinner, 2004). In particular, weakly coupled oscillator theory has been used to predict whether synchronous output could be obtained in electrically coupled networks (Lewis and Rinzel, 2003), and characteristics of phase response curves (PRCs) have been shown to be good predictors of synchronous network output (Pfeuty et al., 2003).

In this paper we aim to determine whether inhibitory networks produce synchronous or asynchronous output when coupled with gap junctions on their active dendrites. We do this using compartmental models, simulations and theoretical insights. We modify our previously developed compartmental model of a hippocampal basket cell (Saraga et al., 2006) in which the dendrites are active, containing voltage-gated channels as is known from experiment (Maccaferri et al., 2004), to express spike attenuation characteristics as experimentally observed. We generate PRCs and use weakly coupled oscillator theory to predict the network output, and find that quantified PRCs can be used as rules of thumb in predicting the synchronous or asynchronous output, which in turn suggests critical cellular characteristics.

2. Results

2.1. Basket cell models

Although there is evidence for voltage-gated channels in the dendrites of hippocampal interneurons (Martina et al., 2000), details as to their densities and distributions are incomplete for basket cells at present. However, it is known that there is an approximately 15% spike attenuation when recordings are performed on dendrites at about 50 μm from the soma with perhaps some differences between basal and apical dendrites (M. Martina, unpublished observations, Maccaferri et al., 2004). We thus built three basket cell models (Cell 1, Cell 2 and Cell 3) with different intrinsic properties such that they exhibit different amounts of basal and apical spike attenuation. This difference is accomplished mainly by varying the sodium channel densities — the channel densities and other cell properties are shown in Table 1. Each model cell has the same morphology and passive properties as used in our previously developed basket cell compartmental model (Saraga et al., 2006; and see Section 4.1), and exhibits spike shape and frequency characteristics of basket cells (see Table 1). In particular, all cells spontaneously fire in the gamma frequency

Table 1 – Model cell characteristics

	Cell 1	Cell 2	Cell 3
Soma g_{Na} (mS/cm ²) ^a	35	45	50
Soma g_K (mS/cm ²) ^a	50	50	50
Apical branch g_{Na} (mS/cm ²) ^a	16	10	8
Apical branch g_K (mS/cm ²) ^a	37.5	37.5	37.5
Basal branch g_{Na} (mS/cm ²) ^a	7	9	10
Basal branch g_K (mS/cm ²) ^a	30	30	30
Average apical branch attenuation (50 μ m from soma)	1.8% \pm 0.3	7.9% \pm 1.0	13.8% \pm 1.9
Average basal branch attenuation (50 μ m from soma)	15.0% \pm 0.2	7.8% \pm 0.2	5.6% \pm 0.1
Spontaneous firing frequency (Hz)	29.8	27.7	30.1
Action potential amplitude (mV)	115	109	101
Afterhyperpolarization (AHP) amplitude (mV)	16	17	14
Resting mean potential (RMP) (mV)	-58	-60	-57

^a Maximal conductances (g_{Na} , g_K) are from conductance-based equations describing ionic currents that are inserted into the multi-compartment model (Eq. (1) in Section 4.1).

range, and exhibit non-negligible afterhyperpolarizations (AHPs). However, Cell 1 has about 15% attenuation on the basal side and much less on the apical side, Cell 2 has about 8% attenuation on both apical and basal sides, and Cell 3 has about 14% attenuation on the apical side and less on the basal side. The model cell characteristics are shown in Fig. 1 for each of the model cells on apical and basal sides. Differences in spike attenuation, spike shape and delays between spikes in the soma and dendrites can be seen between the different model cells.

It is interesting to note that the dendritic sodium channel density is smaller than the somatic sodium channel density for the model cells here. This is different from that found in oriens-lacunosum/moleculare (O-LM) cells and models of them (Saraga et al., 2003). O-LM cells, another type of hippocampal interneuron, spontaneously fire at lower frequencies and play a role in theta oscillations (Klausberger et al., 2003). They do not show as much spike attenuation as basket cells and it is known that they do not have smaller dendritic sodium densities relative to their soma (Martina et al., 2000). However, it is unknown whether gap junctions exist on O-LM cells. We now analyze these basket cell models and examine the behaviour of electrically coupled networks composed of these models.

2.2. Network dynamic groupings of electrically coupled basket cell networks

The phase response curve (PRC) represents an oscillator's response to weak stimuli and can be used to understand collective dynamics via weakly coupled oscillator theory (Ermentrout and Kleinfeld, 2001; Kuramoto, 1984). This powerful theory allows one to say something about the coupled system from the behaviour of the uncoupled system. Furthermore, it has been previously noted that the skewness of the PRC alone, while capturing intrinsic properties of the oscillator, may also be predictive of network properties

(Ermentrout et al., 2001; Gutkin et al., 2005; Pfeuty et al., 2003). Therefore, we (i) apply the weakly coupled oscillator theory to predict network dynamics when two model cells are (weakly) coupled with gap junctions, and (ii) quantify the skewness of our PRCs as a possible predictive measure for the coupled system. Note that our PRCs represent phase advances (positive value) of the somatic spike in response to the stimulus given at a particular dendritic location. Phase zero on the PRC represents the time of the somatic spike peak, and does not necessarily represent the same time as the dendritic spike peak (e.g., see model Cell 3 apical in Fig. 1). We use the simplest possible quantification of the skewness of

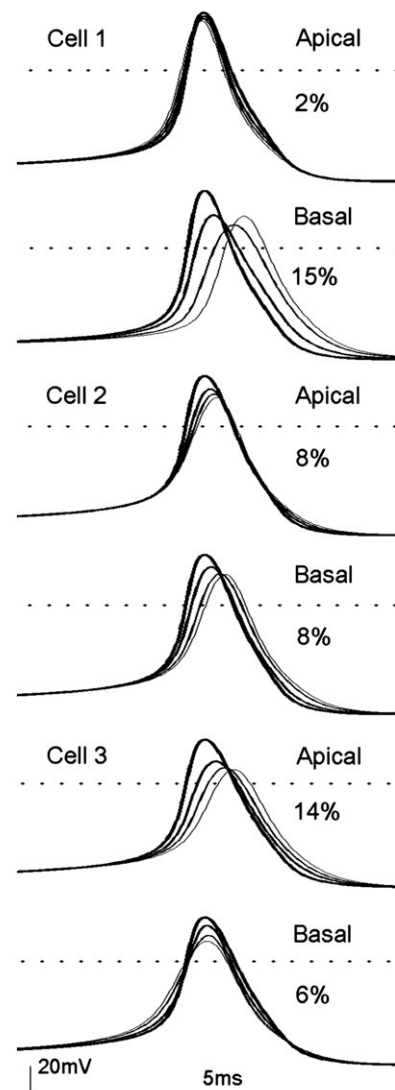


Fig. 1 – Spike characteristics of the model cells. Voltage versus time plots for the three model cells. Somatic and dendritic (50, 150 and 300 μ m) voltages are shown for basal and apical dendrites of each model cell (Cell 1, Cell 2 and Cell 3). Thickest lines refer to somatic voltages and decreasing line thickness to further dendritic locations. Dotted line refers to 0 mV. Note the different spike delays (between soma and dendrite) and spike shapes (AHPs) for the different model cells. Model details are given in Section 4.1 and Table 1.

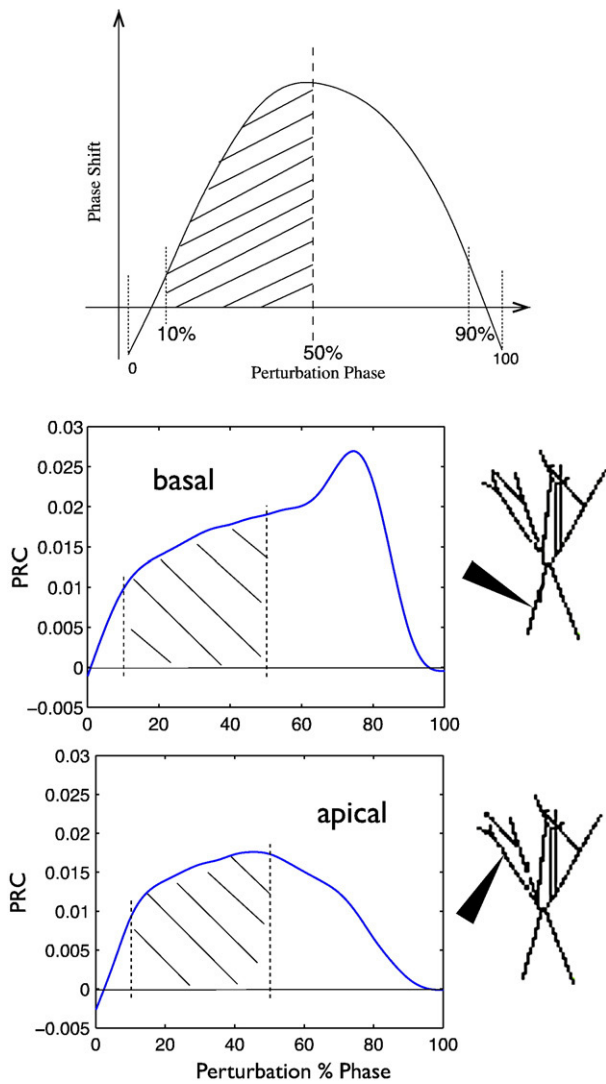


Fig. 2 – Quantifying skewness in phase response curves (PRCs). (Top) Schematic of phase response curve (PRC) illustrating quantification. The x-axis represents the phase at which the perturbation is applied in which the zero value is taken as the peak of the spike at the soma. The y-axis represents the phase shift for the given perturbation with positive values representing a phase advance. The PRC is considered to be left skewed if the shaded area represents more than 50% of the total area under the curve, where the total area is calculated between 10% and 90% perturbation phase. This is done to simplify the consideration of negative phase shifts. We define a “skewness factor” as the % of the total area that the shaded area represents. (Bottom) PRCs for model Cell 3 in which the perturbation (current stimulus) is given either on the apical or the basal dendritic branch located at about 300 μm from the soma as labeled, and as illustrated by the basket cell schematic on the right side. The shaded regions (as described in the top schematic) give skewness factors of 44% (basal) and 58.5% (apical). Stimuli used here are 1 ms duration and 20 pA amplitude.

the PRC by computing the area under the PRC and determining whether the area of the left half is more or less than 50%, i.e., a left or right skew respectively. We call the value obtained for the left area the “skewness factor” and this is illustrated by the shaded area in Fig. 2 (top).

Using different locations (50, 150 and 300 μm) and different apical and basal branches (see model schematic in Fig. 2) of model Cells 1, 2 and 3, we generate PRCs by applying stimuli at different times during the oscillation cycle and compute their skewness factors (see details in Section 4.2). The results for several cases are shown in the second column of Table 2, arranged in ascending order. As an example, the lower two panels of Fig. 2 shows PRCs obtained for model Cell 3 in which either the apical or basal branch is stimulated at about 300 μm from the soma. The different skewness factors obtained, in which there is a left or right skew for basal or apical sides respectively, are apparent.

The theory is applied for the several cases and the predicted phase lags are shown in the third column of Table 2. Briefly, the weak coupling theory involves computing the product of the PRC with a phase-dependent coupling function of the voltage trajectory to give a “Gfcn” from which stable phase-locked solutions are predicted to occur when there is a negative slope at the zero crossing of the Gfcn. Derivation of the Gfcn and further details are given in Sections 4.2 and 4.3. Illustrative plots for the case of model Cell 1 with coupling on the apical branch at about 300 μm from the soma are given in Fig. 3. Specifically, the top plot

Table 2 – Network dynamic groupings

Grouping	PRC skewness factor (%)	Predicted phase lag (%) (weakly coupled oscillator theory)	Computed phase lag (%) (two-cell network simulations with weak coupling, 2–10 pS)	
Syn	41.0	5	1 (10 pS)	
	44.0	7	1 (10 pS)	
	45.2	11	16 (4 pS)	
	48.4	10	1 (10 pS)	
	Asyn	50.3	14	22 (10 pS)
		52.6	16	20 (4 pS)
		52.9	15	21 (4 pS)
		53.7	18	25 (4 pS)
		53.8	19	24 (10 pS)
53.8		19	28 (2 pS)	
53.9	16	23 (4 pS)		
54.2	19	23 (4 pS)		
54.2	18	23 (4 pS)		
54.8	20	23 (4 pS)		
Asyn*	56.8	33	40 (4 pS)	
	57.4	35	37 (4 pS)	
	57.4	50	44 (10 pS)	
	57.5	50	45 (10 pS)	
	58.5	50	44 (10 pS)	
	60.2	50	35 (10 pS)	
	60.7	50	35 (10 pS)	

Computed phase lags using (weak coupling) strengths given in brackets.

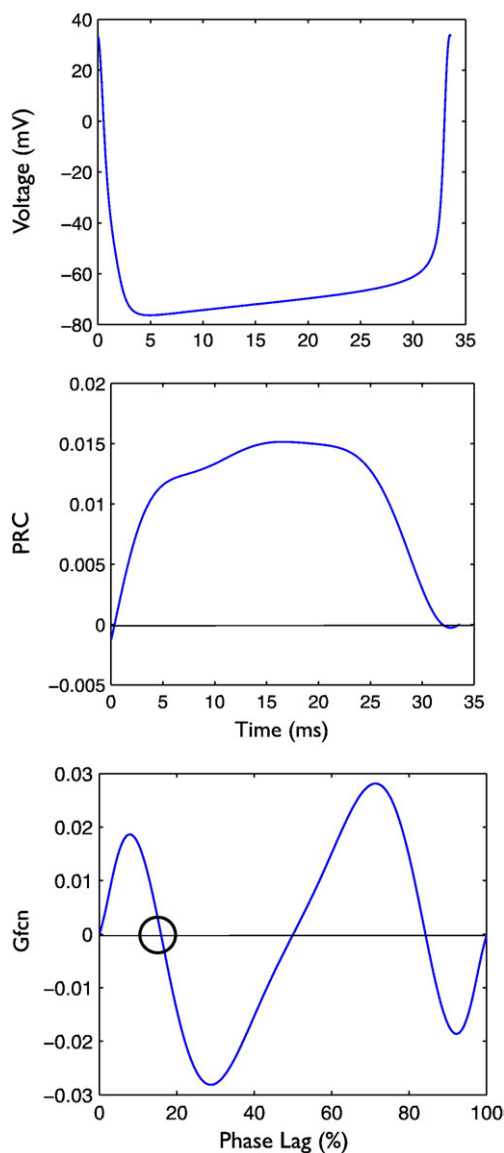


Fig. 3 – Theoretical phase lag prediction illustration. Example voltage, PRC and Gfcn plots for model Cell 1 model. The voltage is for the dendritic site at 300 μm from the soma, and is the location for which the PRC is generated. The bottom plot shows the resulting Gfcn which predicts a stable phase lag of 16%, i.e., where there is a negative slope at the zero crossing. See further details in Sections 4.2 and 4.3.

shows the dendritic voltage trajectory (at 300 μm from the soma) for a single oscillation cycle of the neuron model, the middle plot shows the PRC generated at the same location, and the bottom plot shows the resulting Gfcn from which the stable phase-locked state is predicted to be at 16% phase lag. The predicted phase lags are given in the third column of Table 2. Phase lags are given as a percent of the period.

Examining Table 2 we note that there is a correspondence between skewness factors and predicted phase lags in which larger skewness factors (i.e., more left-skewed) correspond to larger phase lags. Given that the theory uses the PRC in its

calculation to obtain the predicted phase lag, this correspondence is expected, but the correspondence is also expected not to be precise since the PRC alone does not encompass other aspects in the theoretical calculations such as the voltage trajectory (see Section 4.3).

To compare with the theory, two-cell network simulations are done in which the model cells are coupled with gap junctions at the dendritic location for which PRCs were generated and the theory was applied. Weak (2–10 pS) coupling strength values are used to compare with the predicted phase lags from the weakly coupled oscillator theory. An example simulation output is given in Fig. 4 in which two Cell 1 model cells are coupled with 10 pS gap junctions at 300 μm from the soma. Stable phase lags close to that predicted from the theory (as illustrated for the same example in Fig. 3) are obtained. The phase lags obtained from the several simulations are shown in the fourth column of Table 2. We find that our simulation results agree with the predicted values within 10% (see further details in Section 4.3).

Table 2 is arranged in order according to skewness factors and in this way we observe a clear trend in phase lag values. Specifically, there appear to be three groupings of phase lags that can be distinguished. We refer to these as *syn*, *asyn* and *asyn** network dynamic groupings to represent synchronous (close to synchrony), asynchronous, and almost antiphase output from the electrically coupled networks. *Syn* and *asyn** groupings have very different phase lags with the *asyn* grouping having phase lags between the two. We chose to distinguish this third *asyn** grouping since it occurred in many of the simulations and could be neatly separated from the *syn* and *asyn** groupings as shown in Table 2.

We can distinguish these three groupings by examining characteristics of the Gfcn's for the different groups. Sample Gfcn's from the three groupings are shown in Fig. 5. Referring to the first half of the phase lags in the Gfcn plots (the second part is a repeat due to its functional form (see Section 4.3)), we find that for the *syn* grouping, there is a much greater (>3 times) negative amplitude of the Gfcn plot relative to its positive part, and for the *asyn** grouping there is a much greater (>3 times) positive amplitude relative to its negative part. Note that if there is no negative aspect to the Gfcn curve, it is because the antiphase (50% lag) state is stable, as shown in the bottom left plot of Fig. 5. For the *asyn* grouping, there is not a dominance of either positive or negative amplitudes in the Gfcn plot, as illustrated in the top right hand plot. More precisely, we can say that for the *syn* grouping, the Gfcn has negative slope zero crossings close to 0%, for the *asyn** grouping the Gfcn negative slope zero crossings are at 50% or close to it, and for the *asyn* grouping, the negative slope zero crossing is not close to either 0% or 50%.

Given the distinctiveness of these groupings we suggest that one could use skewness values obtained from PRCs as “rules of thumb” to determine whether electrically coupled networks of particular cell types would produce synchronous, asynchronous or close to antiphase patterns. These rules of thumb, based on the results from Table 2, are given in Table 3 where we note that PRC skewness factors less than 50% would be expected to yield synchronous output and

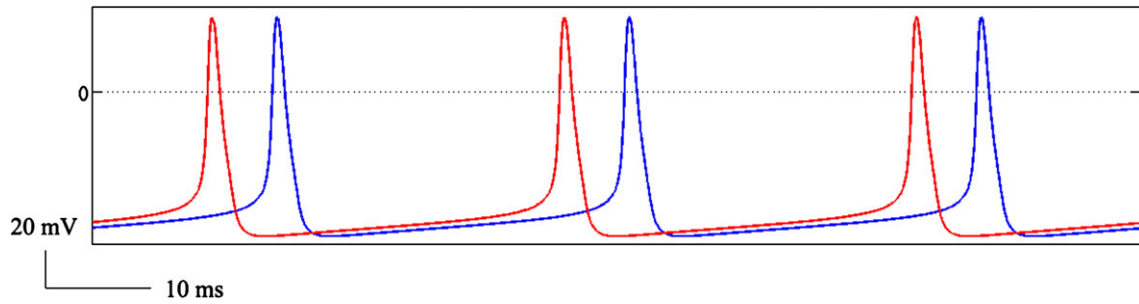


Fig. 4 – Two-cell network simulation illustration. Output from a two-cell network using Cell 1 model neurons, corresponding to the situation shown in Fig. 3. The cells are electrically coupled at their apical dendrites about 300 μm from the soma with a gap junction conductance of 10 pS. The resulting voltage versus time plot shows a stable pattern with a 19% phase lag, close to that predicted from the theory.

those in excess of 55% would be expected to yield antiphase or close to antiphase patterns. We note that while the particular values are specific to the basket cell models used here (although three different models were employed to obtain the values), the presence of three network dynamic groupings is probably more general. Furthermore, since the rules of thumb are based purely on PRCs, they are straightforward to extract from simulations or from experimental data as compared to applying the full theory which also requires computing a phase-dependent coupling function with the voltage trajectory.

2.3. Spike attenuation levels and network groupings

We were able to define three different network groupings based on PRC skewness factors obtained from the individual model cells. Let us now consider these in light of the different intrinsic properties of our three model cells, i.e., their spike attenuation differences. From previous work (Crook et al., 1998; Lewis and Rinzel, 2004; Saraga et al., 2006) we know that the location of gap junction coupling and the particular intrinsic properties of the cell affect whether synchronous output occurs or not. We first note that with more spike

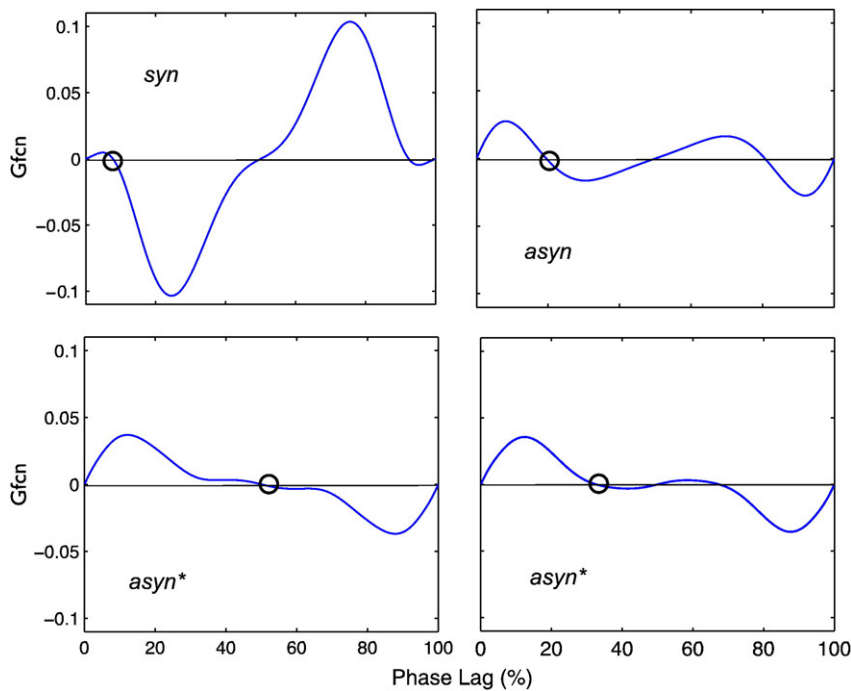


Fig. 5 – Gfncs for the Network Dynamic Groupings Illustrations for the three different network groupings as labeled (syn, asyn, asyn*). Two examples are shown for asyn* in which the antiphase state is stable (bottom left Gfnc plot) or close to the antiphase state is stable (bottom right Gfnc plot). Note the different characteristics of the Gfncs as described in the Results. Syn is for model Cell 3 about 300 μm from the soma on the basal side, asyn is for model Cell 2 about 300 μm from the soma on the apical side, asyn* (left) is for model Cell 3 about 300 μm from the soma on the apical side, and asyn* (right) is also for model Cell 3 about 300 μm from the soma on the apical side but for a different apical dendrite.

Table 3 – Three network dynamic groupings for basket cell models

Grouping	Predicted phase lag	PRC skewness factor
Syn	<12%	<50% (right skewed)
Asyn	12–25%	50–55%
Asyn*	>25%	>55% (left skewed)

attenuation, there is a larger delay in the spike propagation. Thus, for model Cell 1 which has a 15% basal attenuation (see Table 1), there is a 1 ms spike delay on the basal side at 300 μm from the soma, whereas there is only a 0.5 ms spike delay in model Cell 2 (8% basal attenuation) on the basal side at 300 μm from the soma. We also note that the model cells have different AHP characteristics — it is larger in model Cells 1 and 2 relative to model Cell 3 (see Table 1). These different delays and spike characteristics (as can be seen in Fig. 1) are a function of their different intrinsic properties (i.e., voltage-gated channel densities in their dendrites), and give rise to different network outputs.

From previous theoretical work on electrical coupling, it is known that the super-threshold ('spike') component promotes synchronous states whereas the subthreshold part leads to stable asynchronous states (Chow and Kopell, 2000; Gao and Holmes, 2007; Lewis and Rinzel, 2003). This subthreshold aspect, in the form of the AHP size, was shown by Mancilla et al. (2007) to destabilize the antiphase state when decreased (and when the spike width was increased). Thus, stable antiphase states require larger AHP, a subthreshold aspect. Comparing model Cell 3 and Cell 1 basal dendritic voltages at 300 μm , it is clear that the AHP is larger for model Cell 1 (see Fig. 1), and model Cell 1 networks coupled at the basal location give near-antiphase output, whereas model Cell 3 networks coupled at the basal location do not. However, this subthreshold aspect is not a sufficient consideration here — consider model Cell 3 basal and model Cell 3 apical dendritic voltage trajectories, which have similar AHP and spike widths but produce synchronous or asynchronous outputs respectively. The difference in this latter comparison has to do with the spike delay between somatic and dendritic locations (note that the dendritic spike could precede the somatic spike because of its highly active dendrites — this has been seen in experiments with hippocampal interneurons, Martina et al., 2000), in that cells with larger spike delays give asynchronous output in

electrically coupled networks of such cells. On the apical side, model Cell 3 has a larger spike delay between the soma and dendrite relative to the basal side, and for the former comparison, it is also the case that model Cell 1 has a larger spike delay on the basal side relative to that of model Cell 3 on the basal side.

Based on the PRC skewness factor values and the criteria for groupings described above, we can estimate how spike attenuation affects the ability of the network to produce synchronous or asynchronous output. In Table 4 we show PRC skewness factors and their corresponding network grouping, as well as phase lags obtained from network simulations of two model cells coupled to each other at either basal or apical sides approximately 300 μm from the soma. We see that synchronous output occurs when the cells are coupled on the side with little attenuation (small delay), and close to antiphase patterns occur when the cells are coupled on the side where there is larger attenuation. Thus, coupling on the basal side of model Cell 1 or the apical side of model Cell 3 which expresses large enough attenuation (and delay), gives rise to asynchronous patterns and synchronous output is not possible. Using our rules of thumb (Table 3), we can say that if the PRC skewness factor is >55%, we would expect close to antiphase patterns (non-synchronous) to occur in electrically coupled networks of the particular cells at the given location. Given that spike attenuation and/or spike delay are easier to obtain than PRCs in an experimental setting, they could be used to gauge possible network outputs in electrically coupled networks. We note that in other studies with model networks using passive dendrites, computed PRCs indicate that the skewness factor would clearly be greater than 50% and thus correctly predict asynchrony with dendritic coupling (see Fig. 1 in Lewis and Rinzel (2004), and Fig. 10 in Pfeuty et al. (2005)), in line with our observations here. As shown by Goldberg et al. (2007), dendritic PRCs are filtered versions of somatic PRCs and are determined by passive and active properties of the dendrite.

In essence, asynchronous output occurs with larger AHPs (subthreshold aspect), and larger spike delays (somato-dendritic interactions). The former is not captured by PRC characteristics whereas the latter is, as included in how the PRC is defined (see Section 4.2). Therefore, given that the rules of thumb which are based on PRCs are predictive of phase-locking (as shown in the previous Section 2.2, Table 2), this implies that somato-dendritic interactions dominate in

Table 4 – Spike attenuation and network groupings

	Basal			Apical		
	PRC skewness factor (%)	Computed phase lag (%) (two-cell network simulations with weak coupling)	Grouping	PRC skewness factor (%)	Computed phase lag (%) (two-cell network simulations with weak coupling)	Grouping
Cell 1 (2% AA, 15% BA)	60.2	35 (10 pS)	Asyn*	52.6	20 (4 pS)	Asyn
Cell 2 (8% AA, 8% BA)	53.7	25 (4 pS)	Asyn	54.2	23 (4 pS)	Asyn
Cell 3 (14% AA, 6% BA)	44.0	1 (10 pS)	Syn	58.5	44 (10 pS)	Asyn*

BA=basal attenuation, AA=apical attenuation, computed phase lags using (weak coupling) strengths given in brackets.

affecting the resulting network output, and spike delays (which depend on dendritic voltage-gated channel characteristics and where the gap junction is present on the dendrite) are critical factors to consider.

2.4. Networks weakly coupled with multiple gap junctions—same rules of thumb

Let us now consider networks in which gap junction coupling occurs at more than one site as exists anatomically. A single PRC cannot be obtained for multiple site stimulation and so for the PRC to represent a multiply coupled (stimulated) situation and to compute skewness factors, we simply average the PRCs obtained for each of the dendritic sites to produce a single PRC representative of the multiply stimulated situation. The skewness factor is computed using these averaged PRCs and is shown in the second column of Table 5 for model cell networks coupled on apical and basal sides as indicated. To obtain predictions from the weakly coupled oscillator theory, we simply sum the Gfcns from the different sites and obtain the resulting stable phase lags. This is possible to do since the theory essentially uses a linearization around an unperturbed limit cycle so that the superposition principle applies (see Section 4.3 for further details). The PRC skewness factors and predicted phase lags from the theory are shown in Table 5 for doubly and triply coupled networks. Two-cell network simulations with doubly and triply coupled cells with weak electrical coupling yield the phase lag values shown in the fourth column of Table 5. As with the single site coupling scenarios given in Table 2, simulations and predictions agree within 10%. The distinguishable grouping based on the PRC skewness factors are given in the last column of Table 5. Thus our PRC skewness factor rules of thumb are also appropriate for multiply coupled networks.

2.5. Beyond weak coupling

The simulation results discussed so far have been for weak (2–10 pS) gap junction coupling, which would physiologically represent at most a unitary gap junction channel forming the connection. We also perform several simulations that go beyond this weak level to encompass the entire range of physiologically known values. For the cases shown in Table 4

and Table 5, the results are shown in plots of Figs. 6A and 7 respectively. Open symbols refer to cases where the *asyn* grouping occurred for weak coupling, closed symbols refer to when the *asyn** grouping occurred for weak coupling, and starred symbols refer to when the *syn* grouping occurred for weak coupling. For all cases (but note pattern exception below), it is clear that there is a decrease in phase lags as the gap junction coupling strength increases. The phase lag is calculated as a percent of the network period. There is a decrease in the network period with increasing gap junction strength so that it is clear that we are outside the realm of ‘weak coupling’ with the larger strengths — we find about a 5% increase as the largest change in any of the simulations. We also find that as we move beyond the theoretically weak coupling values, multistable patterns emerge. In the simulations, multistability was found by starting the simulations at different initial conditions. In other words, different initial perturbations were used (see Section 4.1). For the single site connections where multistability was specifically found, we indicate this by a star in the plot of Fig. 6A.

In general, the larger the phase lags are with weak coupling (*asyn* and *asyn** groupings) for the given cases, the larger they remain relative to each other as gap junction strength increases when the cells are coupled at a single site. This tendency is also there for the multiply coupled networks but it is possible that this could change with larger coupling strengths (e.g., compare relative phase lags with double coupling at 100 and 1000 pS in Fig. 7). Note that the simulations were done with the same coupling strengths at the different sites but clearly different weightings of coupling strengths would affect the relative phases also.

Although in general phase lags decrease with increasing gap junction strength, synchronous behaviour is not achieved in all cases with the largest physiological gap junction strengths (e.g., see model Cell 1 network coupled at their basal dendrites case in Fig. 6A). However, if there is synchronous behaviour with weak coupling (*syn* grouping), this continues to be the case with increasing coupling strengths. Thus, when *asyn* or *asyn** groupings are present with weak coupling, a wider range of phase lags becomes possible over a physiological range of gap junction strengths. This suggests that the computational capabilities of *asyn*/*asyn** networks are increased since there is an expanded

Table 5 – Multiply coupled cells and network groupings

	Averaged PRC skewness factor (%)	Predicted phase lag (%) (weakly coupled oscillator theory)	Computed phase lag (%) (two-cell network simulations with weak coupling)	Grouping
Cell 1 (2% AA, 15% BA) (1 apical and 1 basal coupled)	55.9	25	29	<i>Asyn</i>
Cell 2 (8% AA, 8% BA) (1 apical and 1 basal coupled)	53.8	18	27	<i>Asyn</i>
Cell 3 (14% AA, 6% BA) (1 apical and 1 basal coupled)	51.5	13	14	<i>Asyn</i>
Cell 3 (14% AA, 6% BA) (1 apical and 2 basal coupled)	49.3	10	1	<i>Syn</i>

BA=basal attenuation, AA=apical attenuation, computed phase lags using 10 pS (weak coupling) strengths.

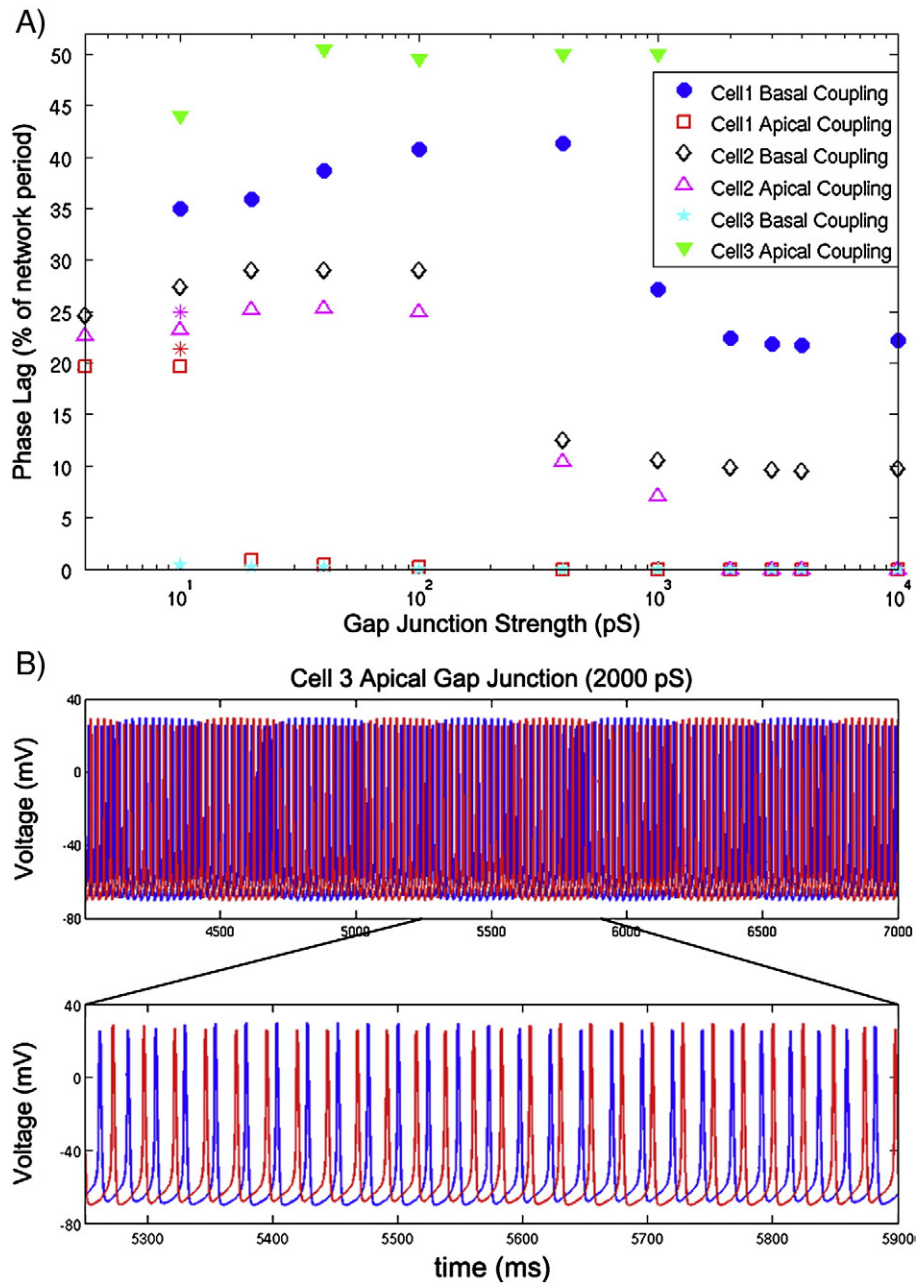


Fig. 6 – Phase lags for networks coupled at a single location for a range of physiological gap junction coupling strengths. (A) Phase lags given as a % of the network period for two-cell networks of Cell 1, Cell 2, and Cell 3 model cells coupled at apical or basal dendrites 300 μm from the soma. If multistability was detected at the 10 pS coupling, then it is indicated with a * symbol. The phase lags decrease with increasing coupling strength as might be expected. For the Cell 3 networks coupled at apical sites, highly non-synchronous activities of anti-phase firing are obtained and increasing the gap junction strength gives rise to an underlying slow oscillation, as illustrated in (B). Note that in all cases there is at most a 5% difference between intrinsic and network periods. (B) Voltage versus time for Cell 3 networks coupled at their apical branches at 300 μm from the soma with a 2000 pS gap junction strength. Top part shows the emergence of an approximately 0.5 Hz modulation in spike amplitudes.

range of phase lag values that can be obtained with modulation of the gap junction strengths.

Interestingly, we find the emergence of a new slow dynamic outside of the weak coupling regime for an *asyn** grouping case — see model Cell 3 apical coupling in Fig. 6A. In this case, the firing remains antiphase as gap junction strength increases and then close to a 2000 pS coupling

strength an additional oscillatory pattern emerges. This is shown in Fig. 6B — the bottom part shows the antiphase firing of the two cells on an expanded scale, and in the top part the slower dynamic is apparent with a switching of the spike amplitude between the cells. It is likely that the emergence of these slow dynamics is related to somatodendritic interactions in the compartmental cells. This is

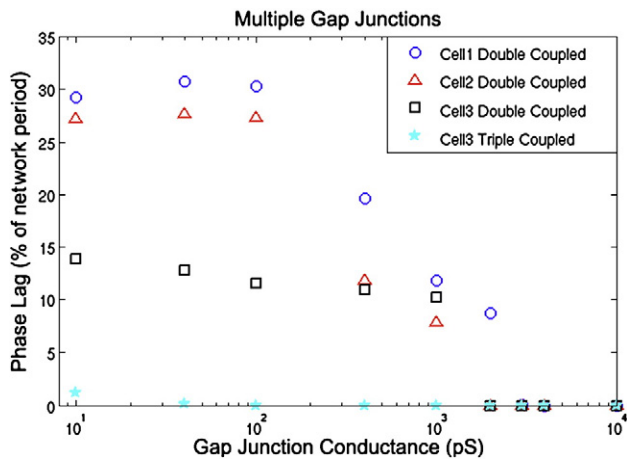


Fig. 7 – Phase lags for networks coupled at multiple locations for a range of physiological gap junction coupling strengths. Phase lags given as a % of the network period for two-cell networks of Cell 1, Cell 2 and Cell 3 model neurons multiply coupled at apical and basal dendrites 300 μm from the soma.

because asynchronous patterns emerge with larger spike delays (somato-dendritic interactions) and, as described above, the spike delay is a critical factor in controlling the network output with weak coupling. In this situation, it may be that the larger coupling used in the simulations is able to push the network to a new stable state in which the spike amplitudes are modulated on a slower time scale.

Our modeling work has shown that the output of (weakly) electrically coupled inhibitory networks can be broken down into three groupings distinguished by their phase lag values as predicted from weakly coupled oscillator theory. Moreover, a quantification of PRCs, which we call skewness factors, can be used as rules of thumb to determine these different groupings. Given this, the spike delay between the soma and dendrite is a critical factor in determining the network output. As shown in simulations that move beyond weak coupling and encompass the range of physiologically relevant values, we find that it is important to be able to differentiate between these different groupings as it affects the way in which the network responds with gap junction modulation.

3. Discussion

In summary, we find that output from networks electrically coupled at their dendrites can be broken down into three different dynamic groupings of synchronous (*syn*), asynchronous (*asyn*) and antiphase-like (*asyn**) patterns, when weakly coupled. Furthermore, we find that values obtained from quantified phase response curves (PRCs) can be used as rules of thumb to distinguish between the three groupings, for singly or multiply coupled networks. For the basket cell models used here, if more than 55% of the area under the PRC curve is to the left, then we expect to get patterns that are antiphase or close to antiphase ($>25\%$ phase lag) in two-cell networks coupled by gap junctions at the dendrite location(s) where the PRC was generated. If less than half the area is to

the left, synchronous behaviour is expected to emerge. These numbers are likely specific to the models used here (although three different models were examined), but the presence of three groupings that can be distinguished by quantified PRCs is probably more general. That PRCs are predictive of the dynamic groupings implies that somato-dendritic interactions critically determine the resulting network output since they influence the PRCs. Thus spike delays (or spike attenuation) are essential factors in affecting network output, with larger spike delays giving rise to asynchronous (near antiphase) output.

We note that network couplings that produce asynchronous (*asyn*, *asyn**) patterns (as opposed to synchronous patterns) with weak coupling encompass more dynamic richness, possibly even leading to more complex patterns (see Fig. 6B). That is, since gap junctions are modulated, an asynchronous output with weak coupling could maximize the range of phase lags that are expressed by the network. Thus if asynchrony with weak coupling is expected based on computed skewness factors of PRCs of particular inhibitory cells, then we would predict that electrically coupled networks of these inhibitory cell types could drastically change their output (between asynchrony and synchrony) with coupling strength changes. These changes could occur with modulation at multiple sites.

3.1. Basket cell networks in hippocampus

In previous work we showed that compartmental models of basket cells endowed with active dendrites expressed network dynamics that could be sensitively tuned by changes in gap junction strengths (Saraga et al., 2006). In general, more active dendrites produced less spike attenuation and less sensitivity in network dynamics with changes in gap junction coupling strengths, staying in the synchronous mode for active dendrites beyond a certain channel density. However, uniform channel densities were used in that work. In our work here, we had different spike attenuations (and intrinsic properties) on basal and apical sides of the model cells. We found that with large enough spike attenuation (or equivalently, large enough delay in spike propagation), asynchronous modes occurred (*asyn/asyn** grouping), and hence more sensitivity with changes in coupling strengths, when dendritic coupling was on the side with large enough spike attenuation. Conversely, if gap junction couplings dominated on the side with less attenuation, synchronous modes would be expected. Fukuda and Kosaka's (2000) anatomical studies indicates a prevalence of gap junction coupling between hippocampal basket cells on the basal side in oriens/alveus layers. If there is also more spike attenuation on the basal side, this would be an indication that basket cells coupled with dendritic gap junctions produce asynchronous output when weakly coupled and thus show sensitivity with changes in gap junction coupling strength. However, basket cells are also coupled with inhibitory synapses which would also play a role in network output.

It has been shown that the stability of the asynchronous state in large networks is related to left skewness of the PRC (Pfeuty et al., 2003). We can interpret our two-cell network results in this light (for *asyn** states). Although the verifica-

tion of (synchrony/asynchrony) model predictions is done using two-cell networks, the relation to quantified PRCs allows our interpretation. The structural organization of the gap junction network has predominantly been examined for PV+ inhibitory cells in hippocampus and neocortex, and they are different for these brain regions (Fukuda, 2007). In hippocampus, the basal dendrites (toward stratum oriens and the white matter) appear to form a continuous lateral network from CA1 to CA3, from CA1 to the subiculum, and also from septal to temporal poles in hippocampus. However, it does not seem to work as a syncytium since the active fraction of the gap junction coupled network (as related to synchrony) is much more limited than the structural numbers. Given that different dynamic patterns are possible in basket cell networks coupled with dendritic gap junctions, it may be that the role of the structural connectivity is to increase the dynamic richness of the output rather than to simply produce synchrony or not.

3.2. Experiments and future directions

To experimentally examine the predictions and insights presented in this work would require dendritic recordings (to obtain PRCs) and dual recordings from interneurons that are electrically coupled to assess their level of synchrony. Assessing the level of synchrony would have to be tempered by the experimental situation — for example, whether a dynamic clamp situation could be used to control and systematically examine the electrical coupling at different dendritic locations, and how much the level of synchrony is influenced by the rest of the network. These would be challenging experiments, especially since they involve dendritic recordings on interneurons. Experimentally derived PRCs have been obtained for neocortical cells and used with weakly coupled oscillator theory to predict network output in electrically coupled cells (Mancilla et al., 2007), assuming somatic gap junction coupling.

One should consider using detailed, compartmental models that are closely linked to experimental data. The basket cell model used here is a start in that direction in which some basket cell characteristics (e.g., spike attenuation) were examined, although some aspects such as spike width are not ideal in the present models. This is not too surprising given that only two types of voltage gated channels are used in the present models. However, more data is becoming available (Hu and Jonas, 2008; Maccaferri et al., 2004; Nörenberg et al., 2008) so that such models may soon be available, and together with sensitivity analysis and optimization approaches (e.g., see Weaver and Wearne, 2008) could lead to robust models. With such models, comparisons of model and experimental dendritic PRCs could be done, and then two-cell model networks used to examine the level of synchrony as predicted in this work. The range and extent of gap junction coupling should be fully examined in the models, and it would be especially interesting to examine and compare differences between apical and basal dendritic couplings since Fukuda and Kosaka's (2000) anatomical studies show that gap junction coupling between hippocampal basket cells may be more prevalent on the basal side in oriens/alveus layers.

Our work has shown that spike attenuation (spike delay) characteristics are critical in determining network output. Simultaneous somatic and dendritic recordings would allow spike delays and attenuations to be measured, and the level of synchrony assessed. For example, as shown in the models here, about a 15% spike attenuation (as measured at 50 μm) is enough to allow asynchronous (antiphase-like) output to occur with gap junction coupling at about a 300 μm location (see model Cell 1 basal and model Cell 3 apical, Table 4). It would be interesting to compare spike delays and attenuations on different apical and basal dendrite locations. Together with robust, compartmental models, predictions of network synchrony would be possible.

It would be further interesting to determine and compare spike delays, attenuations and dendritic PRCs in basket, axo-axonic and bistratified cells, all of which have dendritic gap junctions, as given by their immunoreactivity for Cx36 protein (Baude et al., 2007). Both basket and axo-axonic cells target regions close to the pyramidal cell body. However, unlike basket cells, axo-axonic cells are not coupled with inhibitory synapses. Perhaps axo-axonic cells control synchronous output by gap junction modulation of their networks. If so, we would expect that asynchronous modes with weak coupling are possible (i.e., left skewed PRCs) and large spike delays between soma and dendrites of axo-axonic cells occur. This would allow more flexibility in changing the network output with changes in gap junction strength. It should be noted that both passive and active dendrite properties affect dendritic PRCs (Goldberg et al., 2007) which predict network output. This further motivates obtaining data describing interneuron dendrite characteristics of different interneuron types.

The compartmental models allow one to link experimental parameters (e.g., distribution of sodium channels in the dendrites) that are important in controlling network synchrony. Mathematical reductions that dissect out the dynamics (e.g., see Clewley et al., 2008) could be employed to obtain simpler models that are more amenable to analyses, and thus identify key aspects of control. Analyses would not only provide a deep and thorough understanding of underlying mechanisms, but would also allow larger networks to be computed more easily and interpreted in light of experimental work. Further, theoretical insights from networks that combine inhibitory and electrical coupling (Gao and Holmes, 2007; Lewis and Rinzel, 2003; Pfeuty et al., 2005) could be brought to bear with the simpler models.

From a functional perspective it may be that the gap junction coupled networks bring about cell assemblies that are thought to be the substrate of information coding in the brain (Harris, 2005; Harris et al., 2003). In other words, ramping up and down of gap junction strengths at different multiple sites could be key to the production of cell assemblies. Asynchronous output at weak coupling would be important to allow this range of control. An interesting study regarding patterns of activity in locus coeruleus (LC) and behavioural performance used models and analyses to show that changes in electrotonic coupling among LC neurons could play an important role in attentional modulation (Brown et al., 2004; Usher et al., 1999). It is also of note that large-scale, biophysically realistic models of rat dentate

gyrus indicate the functional importance of non-random connectivity in epileptic brain circuits (Morgan and Soltesz, 2008). Thus, the presence of particular inhibitory cell types coupled with gap junctions inserted with specific connectivities in full-scale networks of hippocampus may be critical for normal and pathological brain states. Examining this in network models which also encompass non-homogeneous couplings could be an interesting avenue to follow.

4. Experimental procedures

4.1. Compartmental models

A 372-compartment model of a hippocampal CA1 basket cell implemented in NEURON (Hines and Carnevale, 1997) was used in this work. The original model, based on a hippocampal basket cell morphology of Gulyás et al. (1999), was constructed by Saraga et al. (2006). This model is available in ModelDB online at <http://senselab.med.yale.edu/ModelDB/ShowModel.asp?model=114047>.

The model is given by the spatially discrete form of the cable equation:

$$C \frac{dV_k}{dt} = \gamma_{k-1,k}(V_{k-1} - V_k) + \gamma_{k+1,k}(V_{k+1} - V_k) - I_{\text{ionic},k} \quad (1)$$

where $C=0.8 \mu\text{F}/\text{cm}^2$ is the capacitance, V is the voltage, t is time, γ is the coupling conductance between connected compartments, I_{ionic} is the ionic current, and k refers to the particular compartment. The axial resistivity, r_L , is $200 \Omega\text{cm}$, and is related to γ such that $\gamma_{i,j}=a/(2 r_L l^2)$ if compartments i and j have the same length (l) and radius (a) (Dayan and Abbott 2001). The compartmental models used here have the same morphology and passive properties used in Saraga et al. (2006), and contain sodium, potassium and leak channels, for which the kinetics were taken from Saraga et al. (2003). That is,

$$I_{\text{ionic}} = I_{\text{Na}} + I_{\text{K}} + g_L(V - E_L) \quad (2)$$

The sodium current, I_{Na} , is described by: $I_{\text{Na}} = g_{\text{Na}}m^3h(V - E_{\text{Na}})$, with

$$\frac{dm}{dt} = \alpha_m(1 - m) - \beta_m m,$$

$$\frac{dh}{dt} = \alpha_h(1 - h) - \beta_h h,$$

where g_{Na} is the maximal sodium conductance, and m and h are the activation and inactivation variables. The reversal potential (E_{Na}) is 55 mV, modified from Saraga et al. (2006). The forward (α_m and α_h) and backward (β_m and β_h) rate constants were found by Saraga et al. (2003) by fitting them to experimentally derived steady state activation and inactivation curves for sodium in the soma and the dendrites:

$$\alpha_{m,s} = \frac{-0.1(V + 38)}{\exp\left(\frac{-(V + 38)}{10}\right) - 1}, \quad \beta_{m,s} = 4\exp\left(\frac{-(V + 65)}{18}\right),$$

$$\alpha_{m,d} = \frac{-0.1(V + 45)}{\exp\left(\frac{-(V + 45)}{10}\right) - 1}, \quad \beta_{m,d} = 4\exp\left(\frac{-(V + 70)}{18}\right),$$

$$\alpha_{h,s} = 0.07\exp\left(\frac{-(V + 63)}{20}\right), \quad \beta_{h,s} = \frac{1}{1 + \exp\left(\frac{-(V + 33)}{10}\right)},$$

$$\alpha_{h,d} = 0.07\exp\left(\frac{-(V + 70)}{20}\right), \quad \beta_{h,d} = \frac{1}{1 + \exp\left(\frac{-(V + 40)}{10}\right)},$$

The potassium current, I_{K} , is described by: $I_{\text{K}} = g_{\text{K}}n^4(V - E_{\text{K}})$, with

$$\frac{dn}{dt} = \alpha_n(1 - n) - \beta_n n,$$

where g_{K} is the maximal potassium conductance, and n is the activation variable. The reversal potential (E_{K}) is -100 mV, taken from Martina et al. (2000). The forward (α_n) and backward (β_n) rate constants are taken from Saraga et al. (2003):

$$\alpha_{n,s} = \frac{-0.018(V - 25)}{\exp\left(\frac{-(V - 25)}{25}\right) - 1}, \quad \beta_{n,s} = \frac{0.0036(V - 35)}{\exp\left(\frac{V - 35}{12}\right) - 1},$$

$$\alpha_{n,d} = \frac{-0.018(V - 20)}{\exp\left(\frac{-(V - 20)}{21}\right) - 1}, \quad \beta_{n,d} = \frac{0.0036(V - 30)}{\exp\left(\frac{V - 30}{12}\right) - 1}.$$

Three different model cells (Cell 1, Cell 2 and Cell 3) are used in this work. They differ only in their maximal sodium and potassium conductances (g_{Na} and g_{K}) in their soma, apical and basal dendrites. The sodium and potassium conductances are uniformly distributed in each apical and basal dendrite.

The reversal potential for the leak channel (E_L) is -60 mV and its conductance, g_L , is $0.0245 \text{ mS}/\text{cm}^2$. The input resistance and membrane time constant of the model is $245 \text{ M}\Omega$ and 30 ms respectively, matching those found experimentally (Morin et al. 1996). The sodium and potassium conductance values are chosen such that they approximately match electrophysiological responses (van Hooft et al. 2000, Morin et al. 1996) and give different spike attenuation values that encompass those seen experimentally (M. Martina, unpublished observations). Spike amplitudes were calculated by taking the difference between the peak of the action potential spike and the minimum voltage following the spike. The afterhyperpolarization (AHP) values were calculated by the difference between the resting membrane potential (RMP) and the minimum voltage following the spike. The RMP value was approximated as the value of the membrane potential before the onset of the action potential, as estimated by the value of the membrane potential at which a doubling of the slope of the membrane potential occurred. Maximal conductance values, spike attenuation values, firing frequency and spike characteristics for the model cells are given in Table 1.

For the two-cell network simulations, non-rectifying gap junctions were added between the dendrites of the two cells. The gap junction current, $I_{\text{gap},k}$, between the k th dendritic

compartments of cell 1 and cell 2, is added to the I_{ionic} Eq. (2), and is given by:

$$I_{\text{gap},k}^1 = g_{\text{gap}}(V_k^1 - V_k^2) \text{ and } I_{\text{gap},k}^2 = g_{\text{gap}}(V_k^2 - V_k^1) \quad (3)$$

for cell 1 and cell 2 respectively.

The network simulations were homogeneous in that the two coupled model cells were the same and the gap junctions were located at the same dendritic site in the two cells — this is reasonable given the structural organization of basket cells in the hippocampus (Fukuda, 2007). At the start of the simulations, a perturbing current was injected into one of the two cells (thus giving different initial conditions) to ensure that the two cells did not fire in synchrony from the beginning.

4.2. Phase-response curve (PRC) computation and skewness factors

The infinitesimal phase response curve (iPRC), $Z(t)$, is given by the normalized phase shift $\Delta\theta_j$ of a cell in response to small, brief current stimulus of amplitude I_{stim} and duration Δt delivered at phase $\theta_j = t + \psi_j$:

$$Z(t + \psi_j) = \frac{\Delta\psi_j}{I_{\text{stim}}\Delta t} \quad (4)$$

PRCs were generated by injecting stimuli (typically 20 pA current for 1 ms duration) into the model cell at different times relative to the oscillation cycle, at dendritic locations where the model cell would be electrically coupled with another model cell in the two-cell network simulations. As is typically done, we assign zero phase as the peak of the somatic spike. That is, zero perturbation phase refers to the input stimulus occurring at the time of the somatic spike peak. Note that since the stimuli are given at dendritic sites, an input stimulus at the somatic spike peak time does not necessarily occur at the same time as the dendritic spike peak time (see Fig. 1). The intrinsic properties of the model cell would affect the relative timing of dendritic and somatic spikes, i.e., how “active” the dendrites are with their voltage-gated channels.

The phase shift of the somatic spike due to the stimulus was measured, normalized for the given stimulus, and plotted to give $Z(t)$, the iPRC, in units of $1/\text{pA}$. Stimuli injections were done at a resolution of 5% of the period. These plots were fit using spline or polynomial curve-fitting in MATLAB. For example, see plots in Fig. 2. These fitted PRCs were used when applying the weakly coupled oscillator theory, and in quantifying the skewness of the PRCs (as described below). Different stimuli ranging from 10 to 75 pA amplitude and 0.5 to 1.5 ms duration were used to ensure that the PRC appropriately represented the neuronal oscillator’s intrinsic properties (not shown).

We quantified the PRCs by calculating the area under the PRC from 10% to 90% of the perturbation (stimulus) phase (as on the x-axis), in order to account for propagation along the dendrite and to simplify consideration of any negative phase shift, and computed the percent of the area that was on the left side of the plot. We refer to this value as the *skewness factor*. When multiple locations of gap junctions are being considered, the average of the various PRCs is used to give a PRC from which the skewness factor is computed.

4.3. Weakly coupled oscillator theory

This theory has been used to analyze networks of neurons (e.g., Crook et al., 1998; Lewis and Rinzel, 2003). Its use lies in its ability to say something about the coupled system using information about the uncoupled system alone. It involves reduction to phase models and computing interaction functions from these reduced models, from which stable phase-locked states can be predicted. The theory and method application is given in detail in Crook et al (1998), Ermentrout (2002) and Lewis and Rinzel (2003).

Here, in deriving the equations, we follow the approach given in Lewis and Rinzel (2003) and Mancilla et al. (2007):

The individual 372-compartment model cell (Eq. (1)) oscillates (i.e., follows a limit cycle) with an intrinsic period, T . This would be the case for each of the 372 compartments in the model. Let V^* represent the uncoupled cell voltage (with a corresponding representation for each compartment). With weak coupling, the system stays on the limit cycle but with small shifts in its phase (i.e., its location on the limit cycle). Thus:

$$V_1(t) \approx V_1^*(t + \psi_1) \dots V_k(t) \approx V_k^*(t + \psi_k) \dots V_{372}(t) \approx V_{372}^*(t + \psi_{372}) \quad (5)$$

for each of the two cells, $i=1,2$.

The gap junction current flowing from cell p to cell q (for the particular dendritic compartment where the gap junction coupling is present) is approximately (see Eqs. (1)–(3)):

$$I_{\text{gap},p \rightarrow q}(t + \psi_q, t + \psi_p) = g_{\text{gap}} [V^*(t + \psi_p) - V^*(t + \psi_q)].$$

Using the PRC and its definition given in Eq. (4), the phase shift in cell q due to the gap junction current (‘stimulus’) from cell p over a brief time Δt is:

$$\Delta\psi_q = Z(t + \psi_q) (g_{\text{gap}} [V^*(t + \psi_p) - V^*(t + \psi_q)]) \Delta t.$$

Rearranging and taking the limit, we obtain:

$$\frac{d\psi_q}{dt} = Z(t + \psi_q) (g_{\text{gap}} [V^*(t + \psi_p) - V^*(t + \psi_q)]).$$

With the weak coupling assumption, the change in phase occurs on a slower timescale than the oscillation period, T , and thus the right hand side of the above equation can be averaged over T .

$$\frac{d\psi_q}{dt} = \frac{1}{T} \int_0^T Z(\bar{t} + \psi_q) (g_{\text{gap}} [V^*(\bar{t} + \psi_p) - V^*(\bar{t} + \psi_q)]) d\bar{t}.$$

With a change of variables, we obtain:

$$\frac{d\psi_q}{dt} = \frac{1}{T} \int_0^T Z(u) g_{\text{gap}} [V^*(u - (\psi_q - \psi_p)) - V^*(u)] du. \quad (6)$$

Rewrite as:

$$\frac{d\psi_q}{dt} = g_{\text{gap}} H(\psi_q - \psi_p) \quad (7)$$

where

$$H(\psi_q - \psi_p) = \frac{1}{T} \int_0^T Z(u) [V^*(u - (\psi_q - \psi_p)) - V^*(u)] du. \quad (8)$$

Let $\phi = \psi_q - \psi_p$ be the phase difference or phase lag between the two cells. Then

$$\frac{d\phi}{dt} = g_{\text{gap}} [H(\phi) - H(-\phi)] \quad (9)$$

and

$$\frac{d\phi}{dt} = g_{\text{gap}} G(\phi) \quad (10)$$

where $G(\phi)$ is a function that includes properties of the uncoupled system: the voltage, the PRC and the expression of the gap junction coupling. Note that the voltage would be the uncoupled voltage at the dendritic location where stimuli are injected to generate the PRC. We will refer to $G(\phi)$ as the Gfcn, and is so specified in the figures. Stable phase-locked solutions, ϕ_{ss} , are present at the zero crossings (i.e., $G(\phi_{\text{ss}}) = 0$) when the slope of the Gfcn is negative at these zero crossings (i.e., $G'(\phi_{\text{ss}}) < 0$). Gfcn's (Eq. (10)) are computed and plotted using a MATLAB code provided by T. Lewis. For example, see Gfcn plots in Fig. 5. The phase lag (ϕ) is given as a % of the period, T , and note that the Gfcn is symmetric about 50% phase lag (or 180°) by virtue of its form $G(\phi) = H(\phi) - H(-\phi)$. Note that identical, symmetrically coupled cells (as is the case here) necessarily exhibit solutions of synchrony and antiphase (0% and 50% phase lags) expressions, although they may not necessarily be stable (Ermentrout et al., 2001; Izhikevich and Ermentrout, 2008). As can be seen in Fig. 5 here and in Lewis and Rinzel (2004, their Fig. 2), although 0% and 50% phase lags exist, they are only sometimes stable.

Due to the small input (weak coupling), the intrinsic dynamics dominate and the system behaves linearly, so that the effect of inputs linearly summate. In other words, the theory essentially uses a linearization around an unperturbed limit cycle (see Eq. (5)). Therefore, if there are multiple couplings at different locations, the different Gfcn's obtained (Eq. (10)) can be summed (superposition principle). For example, for two different locations (different dendritic branches and PRCs), say $G_1(\phi)$ and $G_2(\phi)$ are obtained. For the same coupling strength at the different locations, the resulting Gfcn from which stable phase-locked states are derived is the sum, i.e., $G_{\text{fcn}} = G_1 + G_2$.

It is important to note that the predictions from the theory are only quantitatively accurate for sufficiently weak coupling. In our previous work (Saraga et al., 2006) in which we compared predicted phase lags in a reduced 3-compartment model and computed phase lags in a 372-compartment model, we determined that weak coupling was about 10 pS. Thus, for the studies here, we use this as a starting estimate for weak coupling values (and explore smaller values) to use for the gap junction strengths in our two-cell simulations to compare with the theory. In general, a good comparison (within 10%) with the theory is obtained for 2–10 pS gap junction strengths. This is reasonable considering that one expects some error in

comparison with the theory where the coupling is assumed to be “infinitesimally weak”.

Acknowledgments

We thank F. Saraga for the initial help with the multi-compartment models and NSERC of Canada for funding. We also thank T. Lewis for discussions and for sharing his MATLAB code to perform the Gfcn computations. We thank the reviewers for their many helpful comments that have significantly improved the manuscript.

REFERENCES

- Bartos, M., Vida, I., Frotscher, M., Geiger, J.R.P., Jonas, P., 2001. Rapid signaling at inhibitory synapses in a dentate gyrus interneuron network. *J. Neurosci.* 21 (8), 2687–2698.
- Bartos, M., Vida, I., Jonas, P., 2007. Synaptic mechanisms of synchronized gamma oscillations in inhibitory interneuron networks. *Nat. Rev. Neurosci.* 8, 45–56.
- Baude, A., Bleasdale, C., Dalezios, Y., Somogyi, P., Klausberger, T., 2007. Immunoreactivity for the GABA_A receptor $\alpha 1$ subunit, somatostatin, and connexin36 distinguishes axoaxonic, basket, and bistratified interneurons of the rat hippocampus. *Cereb. Cortex* 17, 2094–2107.
- Brown, E., Moehlis, J., Holmes, P., Clayton, E., Rajkowski, J., Aston-Jones, G., 2004. The influence of spike rate and stimulus duration on noradrenergic neurons. *J. Comput. Neurosci.* 17, 13–29.
- Buhl, D.L., Harris, K.D., Hormuzdi, S.G., Monyer, H., Buzsáki, G., 2003. Selective impairment of hippocampal gamma oscillations in connexin-36 knock-out mouse in vivo. *J. Neurosci.* 23 (3), 1013–1018.
- Buzsáki, G., 2006. *Rhythms of the Brain*. Oxford University Press.
- Chow, C.C., Kopell, N., 2000. Dynamics of spiking neurons with electrical coupling. *Neural Comput.* 12, 1643–1678.
- Clewley, R., Soto-Treviño, C., Nadim, F., 2008. Dominant ionic mechanisms explored in spiking and bursting using local low-dimensional reductions of a biophysically realistic model neuron. *J. Comput. Neurosci.* Jul 2 [Electronic Publication ahead of print] doi:10.1007/s10827-008-0099-1.
- Connors, B.W., Long, M.A., 2004. Electrical synapses in the mammalian brain. *Annu. Rev. Neurosci.* 27, 393–418.
- Crook, S.M., Ermentrout, G.B., Bower, J.M., 1998. Dendritic and synaptic effects in systems of coupled cortical oscillators. *J. Comput. Neurosci.* 5, 315–329.
- Csicsvari, J., Jamieson, B., Wise, K.D., Buzsáki, G., 2003. Mechanisms of gamma oscillations in the hippocampus of the behaving rat. *Neuron* 37, 311–322.
- Dayan, P., Abbott, L.F., 2001. *Theoretical Neuroscience*. MIT Press.
- Ermentrout, B., 2002. *Simulating, Analyzing, and Animating Dynamical Systems: A Guide to XPPAUT for Researchers and Students*. Philadelphia SIAM.
- Ermentrout, B., Kleinfeld, D., 2001. Traveling electrical waves in cortex: insights from phase dynamics and speculation on a computational role. *Neuron* 29, 33–44.
- Ermentrout, B., Pascal, M., Gutkin, B., 2001. The effects of spike frequency adaptation and negative feedback on the synchronization of neural oscillators. *Neural Comput.* 13, 1285–1310.
- Fukuda, T., 2007. Structural organization of the gap junction network in the cerebral cortex. *Neuroscientist* 13, 199–207.
- Fukuda, T., Kosaka, T., 2000. Gap junctions linking the dendritic network of GABAergic interneurons in the hippocampus. *J. Neurosci.* 20, 1519–1528.

- Galarreta, M., Hestrin, S., 2001. Electrical synapses between GABA-releasing interneurons. *Nature Rev. Neurosci.* 2, 425–433.
- Gansert, J., Golowasch, J., Nadim, F., 2007. Sustained rhythmic activity in gap-junctionally coupled networks of model neurons depends on the diameter of coupled dendrites. *J. Neurophysiol.* 98, 3450–3460.
- Gao, J., Holmes, P., 2007. On the dynamics of electrically-coupled neurons with inhibitory synapses. *J. Comput. Neurosci.* 22, 39–61.
- Gloveli, T., Dugladze, T., Saha, S., Monyer, H., Heinemann, U., Traub, R.D., Whittington, M.A., Buhl, E.H., 2005. Differential involvement of oriens/pyramidal interneurons in hippocampal network oscillations in vitro. *J. Physiol. (Lond.)* 562, 131–147.
- Goldberg, J.A., Deister, C.A., Wilson, C.J., 2007. Response properties and synchronization of rhythmically firing dendritic neurons. *J. Neurophysiol.* 97, 208–219.
- Gulyás, A.I., Megias, M., Emri, Z., Freund, T.F., 1999. Total number and ratio of excitatory and inhibitory synapses converging onto single interneurons of different types in the CA1 area of the rat hippocampus. *J. Neurosci.* 19, 10082–10097.
- Gutkin, B.S., Ermentrout, G.B., Reyes, A.D., 2005. Phase-response curves give the responses of neurons to transient inputs. *J. Neurophysiol.* 94, 1623–1635.
- Hajos, N., Palhalmi, J., Mann, E.O., Nemeth, B., Paulsen, O., Freund, T.F., 2004. Spike timing of distinct types of GABAergic interneuron during hippocampal gamma oscillations in vitro. *J. Neurosci.* 24, 9127–9137.
- Harris, K.D., 2005. Neural signatures of cell assembly organization. *Nat. Rev. Neurosci.* 6, 399–407.
- Harris, K.D., Csicsvari, J., Hirase, H., Dragoi, G., Buzsáki, G., 2003. Organization of cell assemblies in the hippocampus. *Nature* 424, 552–556.
- Hines, M.L., Carnevale, N.T., 1997. The NEURON simulation environment. *Neural Comput.* 9, 1179–1209.
- Hormuzdi, S.G., Filippov, M.A., Mitropoulou, G., Monyer, H., Bruzzone, R., 2004. Electrical synapses: a dynamic signaling system that shapes the activity of neuronal networks. *Biochim. Biophys. Acta* 1662, 113–137.
- Hu, H., Jonas, P.M., 2008. Propagation of action potentials in the dendrites of fast-spiking basket cells in the dentate gyrus. Program Number 36.3, 2008 Neuroscience Meeting Planner. Washington, DC: Society for Neuroscience, 2008. Online.
- Izhikevich, E.M., Ermentrout, B., 2008. Phase model. *Scholarpedia*, 3 (10), 1487.
- Klausberger, T., Magill, P.J., Marton, L.F., Roberts, J.D., Cobden, P.M., Buzsáki, G., Somogyi, P., 2003. Brain-state- and cell-type-specific firing of hippocampal interneurons in vivo. *Nature* 421, 844–848.
- Kopell, N., Ermentrout, B., 2004. Chemical and electrical synapses perform complementary roles in the synchronization of interneuronal networks. *Proc. Nat. Acad. Sci. USA* 101 (43), 15482–15487.
- Kuramoto, Y., 1984. *Chemical Oscillations, Waves, and Turbulence*. Springer-Verlag.
- Lewis, T.J., Rinzel, J., 2003. Dynamics of spiking neurons connected by both inhibitory and electrical coupling. *J. Comput. Neurosci.* 14, 283–309.
- Lewis, T.J., Rinzel, J., 2004. Dendritic effects in networks of electrically coupled fast-spiking interneurons. *Neurocomputing* 58–60, 145–150.
- Maccaferri, G., Bartos, M., Lawrence, J.J., LeBeau, F.E.N., Martina, M., Toth, K., 2004. Interneuron diversity and hippocampal network dynamics. Program No. 246. 2004 Abstract Viewer/Itinerary Planner. Washington DC; Society for Neuroscience, 2004. Online (www.sfn.org).
- Mancilla, J.G., Lewis, T.J., Pinto, D.J., Rinzel, J., Connors, B.W., 2007. Synchronization of electrically coupled pairs of inhibitory interneurons in neocortex. *J. Neurosci.* 27, 2058–2073.
- Martina, M., Vida, I., Jonas, P., 2000. Distal initiation and active propagation of action potentials in interneuron dendrites. *Science* 287, 295–300.
- McBain, C.J., Fisahn, A., 2001. Interneurons unbound. *Nat. Rev. Neurosci.* 2, 11–23.
- Meier, C., Petrasch-Parwez, E., Habbes, H.-W., Teubner, B., Güldenagel, M., Degen, J., Söhl, G., Willecke, K., Dermietzel, R., 2002. Immunohistochemical detection of the neuronal connexin36 in the mouse central nervous system in comparison to connexin36-deficient tissues. *Histochem. Cell Biol.* 117, 461–471.
- Morgan, R.J., Soltesz, I., 2008. Nonrandom connectivity of the epileptic dentate gyrus predicts a major role for neuronal hubs in seizures. *Proc. Natl. Acad. Sci. U. S. A.* 105 (16), 6179–6684.
- Morin, F., Beaulieu, C., Lacaille, J.C., 1996. Membrane properties and synaptic currents evoked in CA1 interneuron subtypes in rat hippocampal slices. *J. Neurophysiol.* 76, 1–16.
- Nörenberg, A., Bartos, M., Vida, I., Hu, H., Jonas, P., 2008. Detailed cable models of fast-spiking basket cells in the dentate gyrus. Program Number 36.2, 2008 Neuroscience Meeting Planner. Washington, DC: Society for Neuroscience, 2008. Online (www.sfn.org).
- Parenti, R., Gulisano, M., Zappala, A., Cicirata, F., 2000. Expression of connexin36 mRNA in adult rodent brain. *Neuroreport* 11 (7), 1497–1502.
- Pfeuty, B., Mato, G., Golomb, D., Hansel, D., 2003. Electrical synapses and synchrony: the role of intrinsic currents. *J. Neurosci.* 23, 6280–6294.
- Pfeuty, B., Mato, G., Golomb, D., Hansel, D., 2005. The combined effects of inhibitory and electrical synapses in synchrony. *Neural Comput.* 17, 633–670.
- Saraga, F., Skinner, F.K., 2004. Location, location, location (and density) of gap junctions in multi-compartment models. *Neurocomputing* 58, 713–719.
- Saraga, F., Wu, C.P., Zhang, L., Skinner, F.K., 2003. Active dendrites and spike propagation in multi-compartment models of oriens-lacunosum/moleculare hippocampal interneurons. *J. Physiol.* 552 (3), 502–504.
- Saraga, F., Ng, L., Skinner, F.K., 2006. Distal gap junctions and active dendrites can tune network dynamics. *J. Neurophysiol.* 95, 1669–1682.
- Sherman, A., Rinzel, J., 1992. Rhythmogenic effects of weak electrotonic coupling in neuronal models. *Proc. Natl. Acad. Sci. U. S. A.* 89, 2471–2474.
- Sik, A., Penttonen, M., Ylinen, A., Buzsáki, G., 1995. Hippocampal CA1 interneurons: an in vivo intracellular labeling study. *J. Neurosci.* 15 (10), 6651–6665.
- Skinner, F.K., Zhang, L., Perez Velazquez, J., Carlen, P., 1999. Bursting in inhibitory interneuronal networks: a role for gap-junctional coupling. *J. Neurophysiol.* 81, 1274–1283.
- Söhl, G., Maxeiner, S., Willecke, K., 2005. Expression and functions of neuronal gap junctions. *Nat. Rev. Neurosci.* 6 (3), 191–200.
- Srinivas, M., Rozental, R., Kojima, T., Dermietzel, R., Mehler, M., Condorelli, D.F., Kessler, J.A., Spray, D.C., 1999. Function properties of channels formed by the neuronal gap junction protein connexin36. *J. Neurosci.* 19, 9848–9855.
- Tukker, J.J., Fuentealba, P., Hartwich, K., Somogyi, P., Klausberger, T., 2007. Cell type-specific tuning of hippocampal interneuron firing during gamma oscillations in vivo. *J. Neurosci.* 27, 8184–8189.
- van Hooft, J.A., Giuffrida, R., Blatow, M., Monyer, H., 2000. Differential expression of group I metabotropic glutamate receptors in functionally distinct hippocampal interneurons. *J. Neurosci.* 20, 3544–3551.
- Usher, M., Cohen, J.D., Servan-Schreiber, D., Rajkowski, J., Aston-Jones, G., 1999. The role of locus coeruleus in the regulation of cognitive performance. *Science* 283, 549–554.
- Weaver, C.M., Wearne, S.L., 2008. Neuronal firing sensitivity to morphologic and active membrane parameters. *PLoS Comput. Biol.* 4 (1), e11 Jan, Epub 2007 Dec 13.